Inorganic Chemistry

Article

pubs.acs.org/IC

Synthesis, Structural, and Photoluminescence Studies of $Gd(terpy)(H_2O)(NO_3)_2M(CN)_2$ (M = Au, Ag) Complexes: Multiple Emissions from Intra- and Intermolecular Excimers and Exciplexes

Rylee B. Thomas,[†] Philip A. Smith,[†] Ayesha Jaleel,[†] Paul Vogel,[†] Carlos Crawford,[‡] Zerihun Assefa,*[,‡] and Richard E. Sykora*[,†]

[†]Department of Chemistry, University of South Alabama, Mobile, Alabama 36688, United States

[‡]Department of Chemistry, North Carolina A&T State University, Greensboro, North Carolina 27411, United States

Supporting Information

ABSTRACT: The highly luminescent bimetallic cyanide materials, $Gd(terpy)(H_2O)(NO_3)_2M(CN)_2$ (M = Au, Ag; **GdAu** and **GdAg**, respectively) are quick and easy to synthesize under ambient conditions. A characteristic feature exhibited by both solid-state compounds is an intense red emission when excited with UV light. Additionally, **GdAu** exhibits a broad-band green emission upon excitation in the near UV region. A combination of structural and spectroscopic results for the compounds helps explain the underlying conditions responsible for their unique properties. Single-crystal X-ray diffraction experiments expose their structural features, including the fact that they are isostructural. Crystallographic data for the representative **GdAu** compound (Mo K_α, λ = 0.71073 Å, T = 290 K): triclinic, space group $P\bar{1}$, a = 7.5707(3) Å, b = 10.0671(4) Å, c = 15.1260(4) Å, α = 74.923(3)°, β = 78.151(3)°, γ = 88.401(3)°, V = 1089.04(7) Å^3, and Z = 2. Although the compounds crystallize as dimers containing M···M distances smaller than the sum of their van der Waals radii, the Au···Au (3.5054(4) Å) and/or the Ag···Ag (3.6553(5) Å) interactions are relatively weak and are not responsible for the low energy red emission. Rather, the green emission in **GdAu** presumably originates from the $[Au(CN)_2^-]_2$ dimeric excimer, while the $[Ag(CN)_2^-]_2$ dimers in **GdAg** do not display visible emission at either 290 or 77 K. The unusual red emission exhibited by both compounds likely originates from the formation of an excited state exciplex that involves intermolecular π-stacking of 2,2′:6′,2″-terpyridine ligands. The room-temperature and low-temperature steady-state photoluminescent properties, along with detailed time-dependent, lifetime, and quantum yield spectroscopic data provide evidence regarding the sources of the multiple visible emissions exhibited by these complexes.

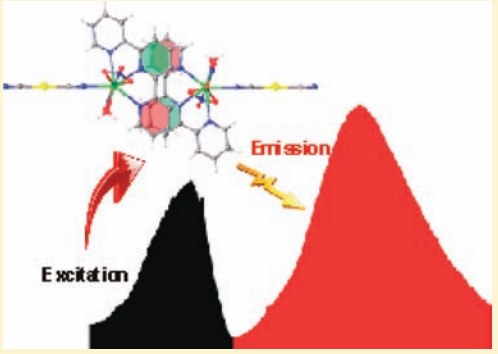

INTRODUCTION

The photophysics and photochemistry of gold(I) continue to fascinate researchers, as evidenced by the large number of topics being discussed recently.[1−7] Dicyanoaurate(I) complexes have been known for a long time but continue to receive interest because of their important scientific[8−10] and industrial applications in fields such as semiconductors,[11] medicine,[12,13] and gold extraction.[14] Of special note regarding these complexes is their unique and interesting photoluminescence (PL) properties.[15] The d^{10}···d^{10} closed-shell interactions are ideal to study in the dicyanoaurates because of the relatively small effect of steric hindrance on the Au(I) centers, which can obscure the extent of these interactions in other systems. A recent development in this area includes the realization of the presence of luminescent M···M bonded excimers and exciplexes in solid-state systems of $[Au(CN)_2^-]_n$, and the related $[Ag(CN)_2^-]_n$ systems.[16,17] Experimental and theoretical evidence both support the prevalence of excited-state interactions in noble-metal systems that contain metal−metal bonds. The optical phenomenon of "exciplex" tuning is one of the characteristic features of dicyanoargentates(I) and dicyanoaurates(I) and entails the tuning of the luminescence spectra to distinct bands characteristic of $[Ag(CN)_2^-]_n$ exciplexes.[16−18]

Although formation of exciplexes is a well-known phenomenon in organic compounds,[19] researchers reported inorganic exciplexes more recently.[20−27] Nagle and Brennan were the first to describe exciplex formation involving a metal−metal-bonded (Pt···Tl) complex in aqueous solutions containing $Pt_2(P_2O_5H_2)_4^{4-}$ and Tl^+.[28] Nagle et al.[29] presented the first report of a luminescent exciplex formed between square-planar d^8 and linear d^{10} ions, as well as the first between like-charged ions in solution, in a system consisting of $Pt_2(P_2O_5H_2)_4^{4-}$ and $Au(CN)_2^-$.

Patterson et al. conducted extensive studies in the d^{10} systems of Ag(I) and Au(I) complexes.[10,16−18,30−32] They showed that it was possible to tune the emission energies of these systems by a variety of physical parameters, including temperature,[31]

Received: July 8, 2011
Published: February 24, 2012

   dx.doi.org/10.1021/ic2014495 | *Inorg. Chem.* 2012, 51, 3399−3408

pressure,[32] excitation wavelength,[17] and dopant concentration.[18] Systems containing Cu(I),[33−36] Ru(II),[25] and Ir(III)[26] provide additional examples of inorganic exciplex formation. Cadmium and mercury are also known to form exciplexes with solvents such as ethers and amines.[27] The exciplex emission bands, a result of the interaction between an excited mercury and the solvent molecules in these compounds, shift to the red as the solvent polarity increases. Systems consisting of an excited mercury atom with a *tert*-butylamine molecule display similar red shifts in some mixed solvents of the amine and alkanes, alcohols, and ethers.[27]

We recently embarked on rationally designing systems where the weak lanthanide emissions can be enhanced through a cooperative effect of multiple donor systems.[37,38] We have ongoing interest in developing synthetic methodologies and spectroscopic properties of systems that contain two or more donor groups attached directly to lanthanide ions. One goal was to target the synthesis of Gd^{3+} complexes containing both 2,2′:6′,2″-terpyridine (terpy) and $Au(CN)_2^-$ donor ligands for comparison purposes with other Ln^{3+} systems since Gd^{3+}, having the largest f−f separation among the lanthanide ions, does not readily act as an energy sink from potential donor groups, such as terpy and $Au(CN)_2^-$. However, adducts containing either $Au(CN)_2^-$ or $Ag(CN)_2^-$, $Gd(terpy)(H_2O)(NO_3)_2M(CN)_2$ (M = Au (**GdAu**), Ag (**GdAg**)), exhibit an unusual luminescence behavior consisting of uncharacteristically bright red emissions. This report describes the details of the synthetic, structural, and photoluminescence studies of these novel complexes.

EXPERIMENTAL SECTION

Materials and Methods. Gd_2O_3 (Alfa-Aesar, 99.999%), 2,2′:6′,2″-terpyridine (Alfa Aesar, 97%), $KAu(CN)_2$ (Alfa Aesar, 99.99%), and $KAg(CN)_2$ (Strem Chemicals, 99.9%) were used for the syntheses as received without further purification. Treating Gd_2O_3 with concentrated HNO_3 and then fuming away the excess acid resulted in the isolation of $Gd(NO_3)_3{\cdot}xH_2O$. The reaction conditions given below produced the highest yields of the respective compounds. A Jasco FT/IR-4100 with a diamond ATR attachment recorded the IR spectra on neat crystalline samples at room temperature in the range 4000−650 cm^{-1}. Galbraith Laboratories, Inc. in Knoxville, Tennessee conducted the CHN analyses.

Synthesis of $Gd(C_{15}H_{11}N_3)(H_2O)(NO_3)_2Au(CN)_2$ (GdAu). The first step in the synthesis of **GdAu** involves mixing a 0.10 M CH_3CN solution of $Gd(NO_3)_3$ (1 mL) and a 0.10 M 20% H_2O:80% CH_3CN solution of $KAu(CN)_2$ (1 mL). After 15 min, a 0.10 M CH_3CN solution of 2,2′:6′,2″-terpyridine (1 mL) is then layered onto the former mixture. Prismatic pale yellow crystals begin to form in less than an hour, and after 24 h the crystals are removed from the mother liquor and washed with methanol. The isolated yield is 80%. IR(solid, cm^{-1}): 3462 (m, br), 2181 (w), 2163 (w), 1662 (w), 1596 (w), 1576 (w), 1521 (m), 1482 (m), 1446 (s), 1431 (s), 1320 (s), 1271 (s), 1263 (s), 1231 (m), 1192 (m), 1169 (w), 1158 (w), 1039 (w), 1023 (m), 1014 (s), 1003 (w), 877 (w), 818 (m), 808 (w), 790 (w), 766 (s), 742 (s), 725 (m), 683 (m), 669 (m). Elemental Analysis Calculated for $C_{17}H_{13}AuGdN_7O_7$: C, 26.13; H, 1.68; N, 12.55. Found: C, 26.33; H, 1.90; N, 12.54.

Synthesis of $Gd(C_{15}H_{11}N_3)(H_2O)(NO_3)_2Ag(CN)_2$ (GdAg). The synthesis of **GdAg** is carried out in a similar manner as described for **GdAu**, except that $KAg(CN)_2$ is used in place of $KAu(CN)_2$. The reaction produces pale yellow single crystals with a yield of 68%. IR (solid, cm^{-1}): 3480 (m, br), 2166 (w), 2155 (w), 1598 (m), 1575 (m), 1507 (m), 1484 (m), 1448 (s), 1433 (s), 1400 (w), 1324 (s), 1277 (s), 1271 (m), 1234 (m), 1196 (w), 1171 (w), 1159 (w), 1041 (w), 1026 (m), 1015 (m), 1005 (w), 820 (w), 768 (s), 743 (m), 727 (w), 677 (w), 669 (w). Elemental Analysis Calculated for $C_{17}H_{13}AgGdN_7O_7$: C, 29.49; H, 1.89; N, 14.16. Found: C, 29.21; H, 1.96; N, 14.06.

Single-Crystal X-Ray Diffraction. Selected single crystals of **GdAu** and **GdAg** with dimensions of 0.37 mm × 0.28 mm × 0.11 mm and 0.20 mm × 0.11 mm × 0.05 mm, respectively, were selected, mounted on quartz fibers, and aligned on a Varian Oxford Xcalibur E single-crystal X-ray diffractometer with a digital camera. Intensity measurements were performed using Mo Kα radiation, from a sealed-tube Enhance X-ray source, and an Eos area detector. CrysAlis[39] was used for preliminary determination of the cell constants, data collection strategy, and data collection control. Following data collection, CrysAlis was also used to integrate the reflection intensities, apply an absorption correction to the data, and perform a global cell refinement.

All materials examined in these studies diffracted extremely well and were nonproblematic in regard to data collection and structure analysis. The program suite SHELX was used for structure solution (XS) and least-squares refinement (XL).[40] The initial structure solutions were carried out using direct methods, and the remaining heavy-atom atomic positions were located in difference maps. The final refinements included anisotropic displacement parameters for all non-hydrogen atoms and isotropic refinements for all H positions. Refinement was performed against F^2 by weighted full-matrix least-squares, and semi-empirical absorption corrections were applied. Crystal data for **GdAu** and **GdAg** are included in Table 1, and select bond distances are listed in Table 2. Additional crystallographic details are available in the Supporting Information. Data can also be obtained free of charge in CIF format by request from The Cambridge Crystallographic Data Centre at www.ccdc.cam.ac.uk/data_request/cif with the CCDC numbers 816045 and 816046 for **GdAu** and **GdAg**, respectively.

Table 1. Crystallographic Data for $Gd(C_{15}H_{11}N_3)(H_2O)(NO_3)_2Au(CN)_2$ (GdAu) and $Gd(C_{15}H_{11}N_3)(H_2O)(NO_3)_2Ag(CN)_2$ (GdAg)

compound	GdAu	GdAg
formula	$GdAuC_{17}H_{13}N_7O_7$	$GdAgC_{17}H_{13}N_7O_7$
fw (amu)	781.56	692.46
space group	$P\bar{1}$ (No. 2)	$P\bar{1}$ (No. 2)
a (Å)	7.5707(3)	7.5255(2)
b (Å)	10.0671(4)	10.0389(3)
c (Å)	15.1260(4)	15.2144(4)
α (deg)	74.923(3)	74.640(2)
β (deg)	78.151(3)	78.914(2)
γ (deg)	88.401(3)	88.880(2)
V (Å^3)	1089.04(7)	1087.08(5)
Z	2	2
T (K)	290	290
λ (Å)	0.71073	0.71073
ρ_{calcd} (g cm^{-3})	2.383	2.116
μ(Mo Kα) (mm^{-1})	9.801	3.979
$R(F_o)$ for $F_o^2 > 2\sigma(F_o^2)^a$	0.0240	0.0153
$R_w(F_o^2)^b$	0.0647	0.0367

$^aR(F_o) = \sum||F_o| - |F_c||/\sum|F_o|$. $^bR_w(F_o^2) = [\sum[w(F_o^2 - F_c^2)^2]/\sum wF_o^4]^{1/2}$

Photoluminescence Measurements. The luminescence spectra were collected using a Photon Technology International (PTI) spectrometer (model QM-7/SE). The system uses a high intensity Xe source for excitation. Selection of excitation and emission wavelengths are conducted by means of computer controlled, autocalibrated "Quadra-Scopic" monochromators which are equipped with aberration corrected emission and excitation optics. Signal detection is accomplished with a PMT detector (model 928 tube) that can work in either analog or digital (photon counting) modes. All of the emission spectra presented are corrected to compensate for wavelength dependent variation in the system on the emission channel. The emission correction files which were generated by comparison of the emission channel response to the spectrum of a NIST traceable tungsten light were used as received from Photon Technology International (PTI). The emission correction was

dx.doi.org/10.1021/ic2014495 | Inorg. Chem. 2012, 51, 3399−3408

Table 2. Selected Bond Distances (Å) for GdAu and GdAg

GdAu		GdAg	
Gd1−O1	2.518(3)	Gd1−O1	2.5192(17)
Gd1−O2	2.483(3)	Gd1−O2	2.4820(17)
Gd1−O4	2.412(3)	Gd1−O4	2.4145(17)
Gd1−O5	2.465(3)	Gd1−O5	2.4748(19)
Gd1−O7	2.386(3)	Gd1−O7	2.3854(16)
Gd1−N1	2.517(4)	Gd1−N1	2.5280(19)
Gd1−N2	2.539(3)	Gd1−N2	2.5465(17)
Gd1−N3	2.528(3)	Gd1−N3	2.5268(19)
Gd1−N4	2.468(4)	Gd1−N4	2.451(2)
Au1−C16	1.988(5)	Ag1−C16	2.047(3)
Au1−C17	1.979(5)	Ag1−C17	2.040(3)
C16−N4	1.128(6)	C16−N4	1.137(4)
C17−N5	1.123(6)	C17−N5	1.133(3)
Au1···Au1[a]	3.5054(4)	Ag1···Ag1[a]	3.6553(5)

[a]Symmetry code: $1-x, -y, -z$.

conducted in real time using the PTI provided protocol. The neutral density filter used in these studies contains an optical density of 1 with 10.0% transmission and a linear response in the 300−800 nm region (series 22000a, Chroma Technology Corp.). The instrument operation, data collection, and handling were all controlled using the advanced FeliX32 fluorescence spectroscopic package. The steady state emission and excitation spectra were collected upon continuous excitation (without introducing any time delay). For the time dependent measurements, various time delays were introduced ranging from 2 to 200 μs. All of the spectroscopic experiments were conducted on neat crystalline samples held in sealed quartz capillary tubes. The low temperature measurements were conducted on samples inserted in a coldfinger dewar filled with liquid nitrogen.

The absolute PL quantum yield (QY) measurements on the solids were conducted using a PTI QM-40, PLQY ultrasensitive fluorimeter system containing a 6-in. integrating sphere (K-Sphere B) redesigned for enhanced measurement of quantum yields of solids, films, and powders. The system includes dedicated quantum yield calculation functions. Wavelength selection is conducted by software controlled excitation and emission monochromators. The QY measurements were conducted on finely ground solids uniformly spread onto the sample holder and covered with a quartz disk.

RESULTS AND DISCUSSION

Syntheses. The reactions of Gd^{3+} solutions with 2,2′:6′,2″-terpyridine and either $KAu(CN)_2$ or $KAg(CN)_2$ in H_2O/acetonitrile mixtures at room temperature lead to the formation of **GdAu** or **GdAg**, respectively. However, we have noted in our studies that the order of mixing of reactants can be crucial to product formation and crystallization. For example, the synthesis of **GdAu** involves the mixing of the Gd^{3+} and dicyanoaurate solutions followed by layering of the 2,2′:6′,2″-terpyridine solution. Crystals of $[Gd(terpy)(H_2O)_3(NO_3)_2]$-$NO_3$[41] begin to form within minutes if the $Gd(NO_3)_3$ and 2,2′:6′,2″-terpyridine solutions mix prior to the addition of the dicyanoaurate(I) solution.

Structural Studies. In the quest to develop the concept of dual-donor sensitization phenomena, our groups have been involved in combining tetracyanoplatinates (TCP) with selected organic donor ligands for enhancement of the lanthanide ion sensitization.[37,38] In the current work, we have expanded to include the group 11 dicyanometallates, $Au(CN)_2^-$ and $Ag(CN)_2^-$. Our initial aim was to investigate whether weak lanthanide emissions could be enhanced through a cooperative effect when one of the donor systems involves a group 11 cyanide directly bonded to the lanthanide ion. Synthetically, the linear $Au(CN)_2^-$ or $Ag(CN)_2^-$ donors easily replace the TCP unit, but drastic structural changes take place. A molecular structure for **GdAu** and **GdAg** results, rather than the coordination polymeric features exhibited in several Ln^{3+}/terpy/TCP systems.[37,38] In the former, the Gd^{3+} ion contains one terpy ligand, two bidentate NO_3^- anions, one H_2O molecule, and one $[M(CN)_2]^-$ (M = Ag, Au) anion, as seen in Figure 1, providing a total coordination number of nine for Gd^{3+}. The environment around Gd^{3+} contains a geometry best described as a distorted $[GdO_5N_4]$ tricapped trigonal prism.

Table 2 displays a list of select bond distances for **GdAu** and **GdAg**. The Gd−N and Gd−O bond distances range from 2.451(2) to 2.546(2) Å and 2.385(2) to 2.519(2) Å, respectively. The longest Gd−O bond distances are those to the nitrate anions (average of 2.471 Å), while the Gd−O distances to the coordinated water molecules are considerably shorter (2.386 Å average). A distinction in the distances for the Gd−N bonds to the dicyanometallate groups and the Gd−N bonds to the terpyridine moiety is also evident; the Gd−N bonds to the latter are longer by ∼0.07 Å on average. The Au−C and Ag−C distances have averages of 1.984(5) and 2.044(3) Å, consistent with past structural studies on dicyanometallates.[30a] The C−N distances for the terminal and bridging cyano groups are the same, within error.

The structural diagram of **GdAu**, shown in Figure 1, reveals that two molecules related by an inversion center are held together by a combination of hydrogen bonds and a metallophilic, Au···Au or Ag···Ag, interaction. The H bonds are not extraordinary, and their geometries are included in the CIF file of the Supporting Information. The M···M interactions in **GdAu** (3.5054(4) Å) or **GdAg** (3.6553(5) Å) are several tenths of an angstrom longer than observed in $Gd[Au(CN)_2]_3\cdot 3H_2O$ (3.3221 Å) or $Gd[Ag(CN)_2]_3\cdot 3H_2O$ (3.3403 Å Ag···Ag

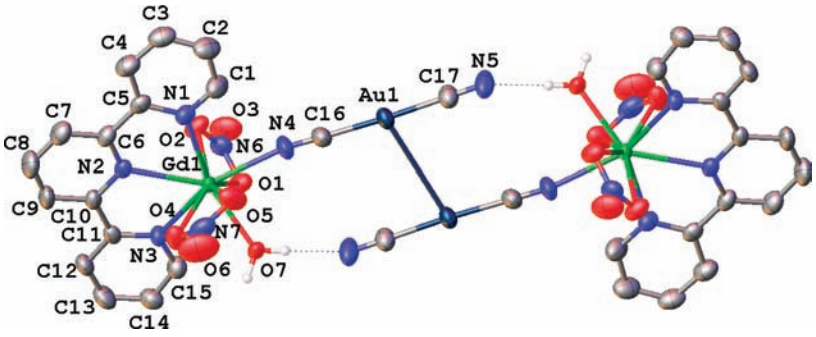

Figure 1. A thermal ellipsoid plot (50%) of **GdAu** illustrating the coordination environment of the Gd^{3+} site and the dimers formed from the H-bonds and Au···Au interaction. **GdAg** is isostructural with **GdAu** and therefore contains the same arrangement of atoms.

dx.doi.org/10.1021/ic2014495 | Inorg. Chem. 2012, 51, 3399−3408

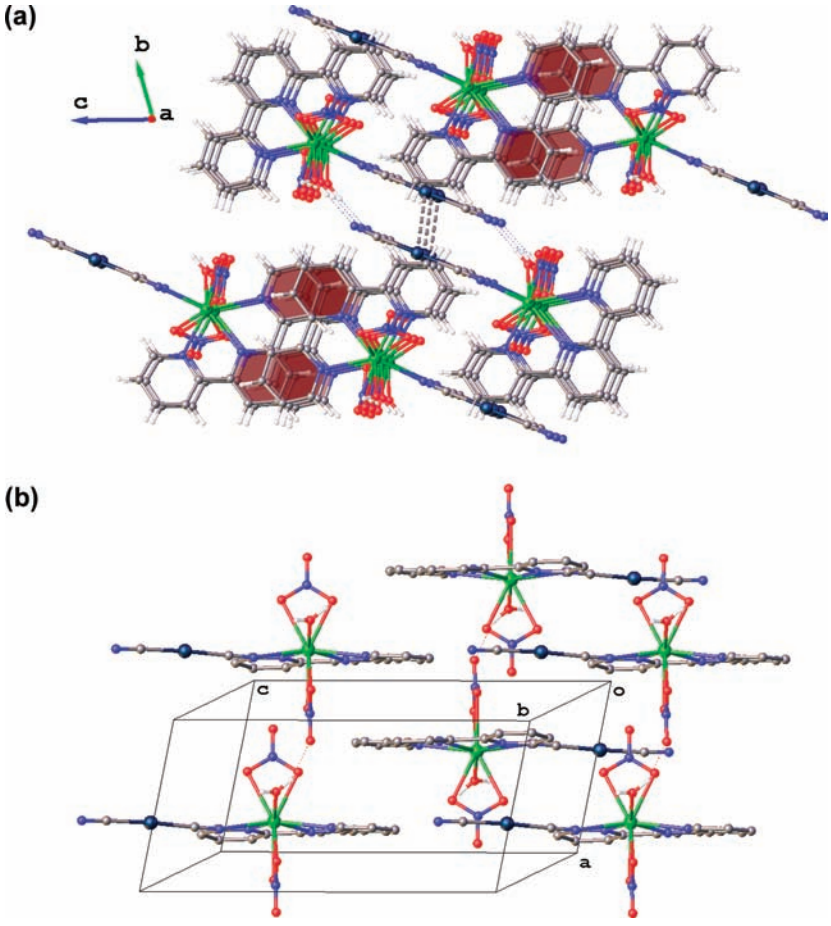

Figure 2. (a) A packing diagram for **GdAu** viewed along the *a* axis highlighting the π-stacking between the 2,2′:6′,2″-terpyridine ligands which are located in the *bc* planes. The partially overlapping rings are highlighted for clarity, and the Au···Au interactions are showed with dashed lines. (b) A packing diagram viewed perpendicular to the π-stacking interactions. Intermolecular H bonds between O−H (H_2O) donors and oxygen (NO_3^-) acceptors are also shown.

distance).[42] These distances are also consistent with the widely observed feature that Au···Au interactions are typically shorter than Ag···Ag interactions in isostructural compounds, due to the smaller size of Au^+ relative to Ag^+.[43h]

$Gd[Au(CN)_2]_3{\cdot}3H_2O$ and $Gd[Ag(CN)_2]_3{\cdot}3H_2O$ have two-dimensional kagome sheets of metal atoms that form a long-range network of M···M interactions. This arrangement is notably different from that observed in **GdAu** and **GdAg**, where the dimeric units formed in the structures only contain one isolated M···M interaction, a consequence of the disruption of the formation of the higher dimensional M···M bonding by the incorporation of the chelating ligands (terpyridine and nitrate) into these structures. Several recently reported lanthanide tetracyanoplatinate systems[37,38] show a similar reduction in the dimensionality of their Pt···Pt interactions. While many known tetracyanoplatinates contain quasi-one-dimensional stacks (also described as chains) of tetracyanoplatinate anions, the incorporation of an ancillary ligand such as 2,2′:6′,2″-terpyridine results in the disruption of these stacks and subsequent isolation of Pt_2 dimers.

A characteristic feature observed in the packing arrangement of **GdAu** and **GdAg**, shown in Figure 2, is the presence of partial ring alignment of the terpy groups along the *a* axis with an average interplanar distance of 3.522 Å. The dimeric Au···Au axis is canted 68.4° relative to the average plane of each terpy ligand and not closely associated with the pyridine rings involved in π-stacking. Both the π-stacking and aurophilic interactions, and their uncoupled nature, prove to have an important consequence on the spectroscopic properties of the compounds, as described in detail below.

Photoluminescence (PL) Studies of GdAu at Room Temperature. The emission properties of **GdAu**, shown in Figure 3, display excitation dependent behavior. When excited at 364 nm, the compound exhibits a broad, intense band covering the 500−750 nm region with an emission maximum at ~612 nm.

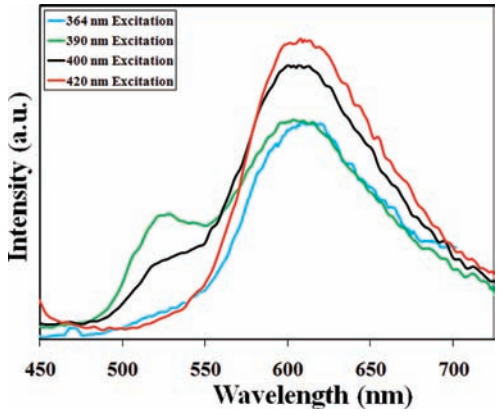

Figure 3. Room-temperature emission spectra of **GdAu** as a function of excitation at 364, 390, 400, and 420 nm.

dx.doi.org/10.1021/ic2014495 | *Inorg. Chem.* 2012, 51, 3399−3408

Changing the excitation radiation to longer wavelengths provides a distinct emission peak at ~525 nm, whose intensity maximizes at an excitation wavelength of ~390 nm. A further shift to longer wavelengths, however, provides a decrease in the intensity of the 525 nm peak, which totally disappears when the excitation wavelength reaches ~420 nm. The intensity of the red-orange emission band increases concomitantly with the shift of the excitation to longer wavelengths, with the maximum intensity obtained at ~428 nm excitation.

The influence of the excitation wavelength on the emission profile is more evident in Figure 4. When monitored at 612 nm,

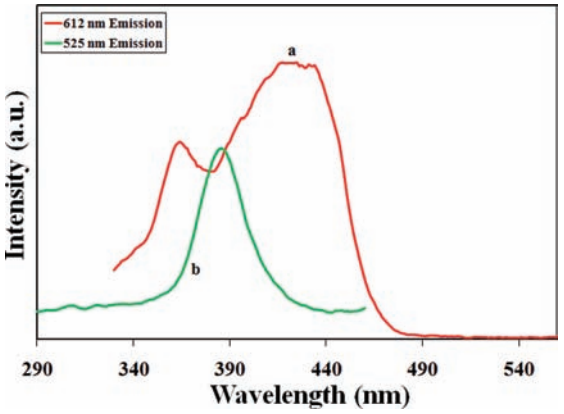

Figure 4. Room-temperature excitation spectra of **GdAu** monitored at (a) the 612 nm (red) and (b) the 525 nm (green) emission band.

the excitation spectrum of **GdAu** (Figure 4a) shows a broad band with maxima at 365 and ~425 nm and sharply falls on the low energy side of the spectrum. Shifting the monitoring wavelength to 525 nm, however, results in an entirely different excitation profile, one in which a much sharper excitation band maximizes at 387 nm (Figure 4b). The spectral profiles clearly indicate that the two luminescent moieties are uncoupled and behave as if they originate from two different chemical species within the compound operating independently. Reproduction of these spectral results on multiple X-ray-quality crystals, from numerous preparations, indicates that an impurity mode is not responsible for the behavior; rather, the system contains multiple uncoupled excited states. Similarly, (TPA)AuBr (TPA = triaazaphosphaadamantane)[44] displays distinct emission bands, resulting from two uncoupled excited states.

PL Studies of GdAu at Low Temperature. The overall spectral features of **GdAu** exhibit a significant increase in complexity, as shown in Figure 5, when measured at 77 K. When the excitation wavelength is between 400 and 450 nm, the broad low-energy emission maximizes at ~580 nm, a blue shift by 900 cm^{-1} when compared with the room temperature data. In addition, as is the case with the room temperature spectrum, a well-defined band is observed at 530 nm (a small red shift when compared with the room temperature data).

However, when the excitation wavelength is below 400 nm a drastic change in the emission profile takes place. For example, with an excitation wavelength of 386 nm, the emission maximum blue shifts to shorter wavelengths, and structured bands are observed at 466.5, 502.5, 530, 561, and 610 nm (Figure 5b). The average spacing is ~1300 cm^{-1}, suggesting vibronic coupling of the terpy group involved in these transitions. A further shift of the excitation wavelength to 300 nm provides an entirely different structured emission at much shorter wavelengths of 356,

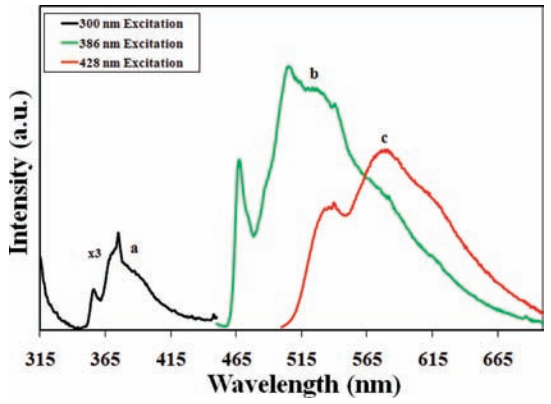

Figure 5. Low temperature (77 K) emission spectra of **GdAu** which illustrate the wavelength dependence upon excitation at (a) 300 nm (black), (b) 386 nm (green), (c) 428 nm (red).

375, and 390 nm with an average spacing of ~1220 cm^{-1}. Again, this spacing is similar to the emission profile obtained from the 386 nm excitation and indicates the terpy ligand involvement in the transition.

Overall, as shown in Figure 5, the profile covers spectral bands ranging from 350 to 700 nm, attributable to the presence of multiple emitting states in this system. Observation of emission bands tuned simply by changing the excitation wavelength, over a broad range of wavelengths, is *unusual and reported in only a few instances thus far.*[17,33]

The low-temperature excitation behavior of the **GdAu** system is also quite complex, as shown in Figure 6. When monitored at the 612 nm emission band, a poorly resolved broad excitation profile is obtained as shown in Figure 6a, whereas a well structured and relatively sharper band is observed when monitored at the most intense band at 500 nm (Figure 6c).

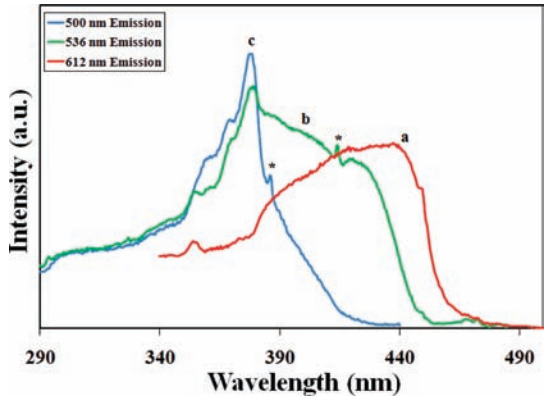

Figure 6. Low temperature (77 K) excitation spectra of **GdAu** monitored at (a) 612 nm (red), (b) 536 nm (green), and (c) 500 nm (blue). Ghost peaks are labeled with an asterisk.

The average spacing of ~590 cm^{-1} is much smaller than the spacing obtained in the emission profile, suggesting that the excited state in this system involves vibronic coupling other than the terpy ligand. The excitation spectrum monitored at 536 nm (Figure 6b) consists of a combination of the two features discussed above where the higher energy side displays the structured feature prominent in Figure 6c, while the lower energy side resembles the feature prevalent in Figure 6a.

PL Studies on the GdAg System. Figure 7a shows the PL spectra of the **GdAg** system measured at room temperature.

dx.doi.org/10.1021/ic2014495 | *Inorg. Chem.* 2012, 51, 3399–3408

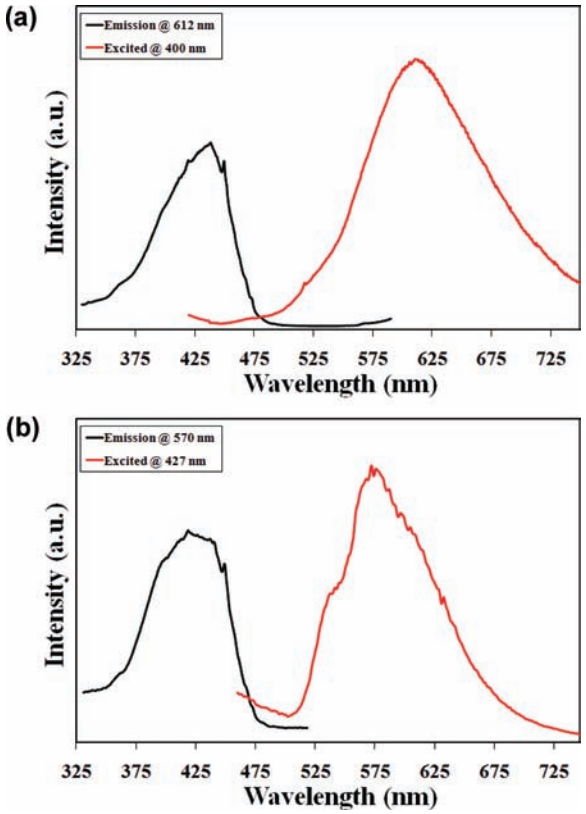

Figure 7. Excitation and emission spectra for **GdAg** measured at (a) room temperature and (b) 77 K.

The observance of a broad red-orange emission centered at ~615 nm covering the 530−750 nm region is the main feature of this spectrum. At 77 K, the emission maximum blue shifts by ~1200 cm^{-1} and is observed at 570 nm, as can be seen in Figure 7b. A well-defined broad shoulder is also evident at 535 nm. In contrast, the excitation spectrum at 77 K red shifts only by ~540 cm^{-1} and maximizes at 440 nm, as compared with the 430 nm maximum observed in the room temperature spectrum.

Comparison of the Low Energy Emission in GdAu vs GdAg. As mentioned earlier, a common feature observed in the **GdAu** and **GdAg** systems is that both compounds display a broad orange-red emission under UV excitation. Observance of a similar PL property in both Au and Ag based compounds has been unusual and intriguing for several reasons. First, although Gd^{3+} is the common metal ion in both complexes, the broad emission at ~600 nm cannot be related with an f−f transition. Second, the band also cannot be assigned to gold-centered (MC) emission of the cyanometallates, since the large M···M distances in these systems are expected to provide relatively higher energy emissions. Only short Au···Au distances of <3.1 Å are known[44−46] to result in metal-centered red emission. The Ag···Ag separation in **GdAg**, which is slightly larger than the summed van der Waals radii of two silver atoms (3.4 Å), should show weak ground state Ag···Ag interactions and, hence, is an unlikely source of the low energy red-orange emission. It is interesting to note that in the series of isostructural Ln^{3+}/dicyanometallate/terpyridine systems studied so far,[42] the red-orange emission is unique for the Gd^{3+} systems, **GdAu** and **GdAg**.

Assigning this low energy band to a ligand centered emission (LC) has also been discounted initially, based on previous reports where the terpy ligand exhibited an intense violet luminescence in acidic aqueous solution.[47−49] However, this assertion has been re-evaluated, as will be discussed in the next section.

The Low Energy Band and Exciplex/Excimer Model. Close analysis indicates that the overall spectral profile of the low energy emission is consistent with the criteria needed for an excimer/exciplex model common in planar aromatic compounds such as pyrene.[19,50] In these systems, broad, structureless, and long-lived emissions with large Stokes shifts are commonly observed. These properties are typical of exciplex features, as they indicate a very large displacement of the excited state relative to the geometry of the ground state.

Known structural requirements for excimer formation in solid-state organic compounds include the presence of stacking or pairing of molecules with interplanar distances of less than 3.5 Å.[51] The structural features exhibited in **GdAu** and **GdAg** appear to support this assertion since the terpy groups, although not perfectly stacked as shown in Figure 2, show partial ring alignment along the *a* axis with average interplanar distances between the rings of 3.522 Å. The structural features described earlier indicate that two molecules are held together by a combination of two hydrogen bonds and one Au···Au (or Ag···Ag) interaction. Although this is in fact the case, the M_2 dimeric units are not closely associated with the π-stacking interactions of neighboring terpyridine units and are therefore electronically isolated. Hence, the compound exhibits a unique situation where, on one side, two molecules related by an inversion center are held together through the metallophilic and H-bonding interactions. On the other hand, intermolecular π-stacking interactions persist, but the metallophilic and π-stacking interactions are not structurally coupled.

Structural analysis of known terpy containing complexes indicates that π-stacking is not unique for the **GdAu** and **GdAg** systems. For example, the packing diagram of [terpyH]-CF_3SO_3[48,52a] contains planar terpy moieties aligned parallel to each other and stacked with sets of parallel planes held together by extensive hydrogen-bonding and strong dipole−dipole interactions. The planar arrays have distances of 3.135 Å. However, in the structure of a related compound with an alternate counteranion, [terpyH]PF_6, the stacking feature is random with a dihedral angle of 60.9°.[48]

These observations indicate that certain factors *might be essential in contributing to stacking features*. One such factor was found to be the position of protonation at either the terminal pyridine N atoms or the central pyridine ring site. In [terpyH]-CF_3SO_3,[48,52a] for example, the terminal pyridine group is protonated, leading to stacking, while in [terpyH]PF_6,[48] the central pyridine group is protonated. This latter observation suggests that H-bonding interactions may also play an important role in the formation of strong π-stacking interactions in these compounds.

The spectral profile in these systems is also dependent on the position of ring protonation and by inference the mode of coordination with metal ions. Accumulated data[48,52] on the terpy ligand indicates that protonation red shifts the absorption bands due to the formation of a more planar geometry, leading to extension of the π delocalization when compared with the typically nonplanar unprotonated moiety. We have also investigated the solution spectral properties on the doubly recrystallized terpy ligand, where a significant red shift was observed in aqueous acidic media relative to the spectral profile in acetonitrile (550 vs 438 nm, respectively). Two absorption

dx.doi.org/10.1021/ic2014495 | *Inorg. Chem.* 2012, 51, 3399−3408

bands are also evident, centered at 280 nm with a shoulder at 330 nm, consistent with a previous report.[53]

Additional support for the exciplex/excimer assignment in **GdAu** and **GdAg** is presented in the emission spectrum of $[Gd(terpy)(H_2O)_3(NO_3)_2]NO_3$, **Gd(terpy)**, shown in Figure 8.

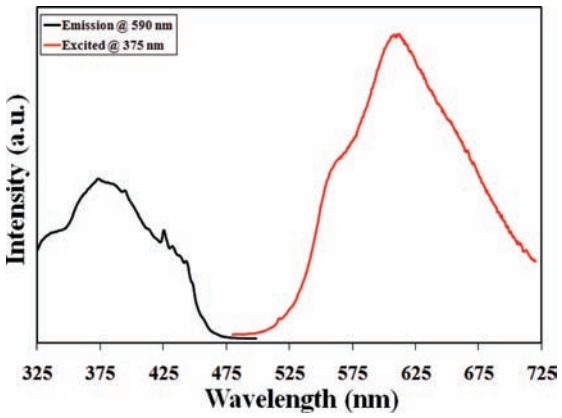

Figure 8. Room temperature excitation and emission spectra for **Gd(terpy)**.

In some ways, this compound displays a quite similar profile to that of the **GdAu** and **GdAg** systems, which would not be expected if the dicyanometallates were playing a dominant role in the spectroscopic properties of these compounds. The room temperature spectrum of **Gd(terpy)** reveals a broad emission band that maximizes at 606 nm with a shoulder at 556 nm. When measured in liquid N_2 (Figure S1), the band maximum slightly blue shifts to 593 nm. Similarly, the excitation band maximizes at 370 nm at room temperature and red shifts by 1450 cm^{-1} and maximizes at 390 nm at 77 K. The lifetime of **Gd(terpy)** measured at 600 nm is 1.12 ms, with a similar value also observed at 525 nm (1.1 ms, Table 3). Interestingly, similar

Table 3. Luminescence and Photophysical Data for GdAu, GdAg, and Gd(terpy)

compound	λ (nm)	ϕ_{sp}	τ, μs	k_r, s^{-1}	k_{nr}, s^{-1}
GdAu	600	0.027	1525	17.7	6.38×10^2
GdAu[a]	525		130		
GdAg	600	0.109	1290	84.4	6.85×10^2
Gd(terpy)	600		1120		
Gd(terpy)	525		1090		

[a]The QY could not be measured accurately due to significant overlap with the 600 nm emission band.

lifetimes of 1.5 and 1.3 ms were obtained for the **GdAu** and the **GdAg** emission, respectively, measured at 600 nm. However, the emission lifetime for **GdAu** measured at the 525 nm shoulder is shorter by a factor of about 10 relative to the comparable band in **Gd(terpy)**, which shows a lifetime identical to the lower energy 600 nm broad band.

The lifetime difference in the two bands is more pronounced in the time dependent profiles shown in Figure 9 for the three compounds. **GdAu** and **GdAg** have a common feature in that, at shorter time delays, the higher energy band dominates, while at longer delay times, only the low energy band is dominant. Hence, at delay times of up to 20 μs, only the 525 nm emission emerges. In contrast, the band at 600 nm is dominant at delay times of 100 μs and above. In the **Gd(terpy)** system, however,

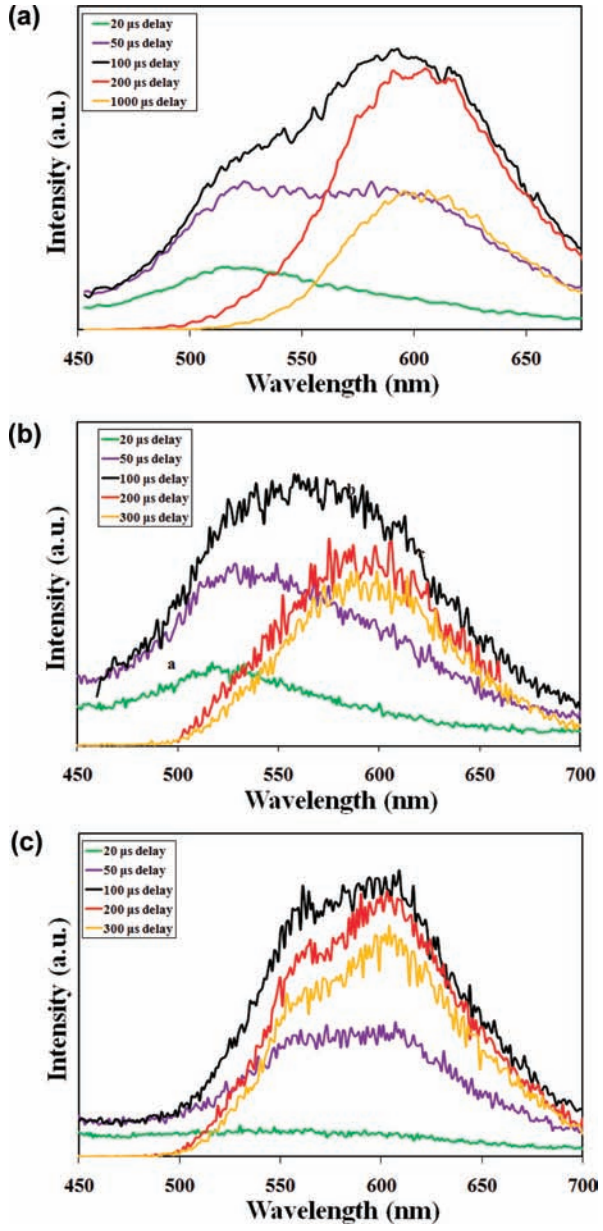

Figure 9. Time dependent emission spectra, collected upon excitation at 360 nm, for (A) **GdAu**, (B) **GdAg**, and (C) **Gd(terpy)** collected after various time delays.

the spectral profile does not change with delay times other than an overall variation in intensity. Hence, the band at 600 nm and the shoulder at 550 nm are in a similar ratio at all delay times (Figure 9C), as expected from the lifetime data. These results are consistent with our interpretation that the low energy band in all three compounds originates from the common feature of π-stacking induced exciplexes involving the terpy ligand, similar to those observed in pyrene.

A standard kinetic model of the intermolecular excited-state complex (excimer) formation involves association of an excited molecule with a ground state molecule followed by the breakup of the excited complex and its return to the ground state through radiative and nonradiative processes. The full understanding of the kinetic processes requires knowledge of the radiative and nonradiative rate constants, the excimer dissociation rate, and the rate of excitation energy transfer to the excimer sites, in addition to an estimate of the fraction of

dx.doi.org/10.1021/ic2014495 | Inorg. Chem. 2012, 51, 3399–3408

chromophores involved in excimer formation. Additional studies in these areas are currently underway and are beyond the scope of this report.

High Energy (HE) Emission Band Assignment. While the low energy emission has been assigned to the formation of a stable exciplex product in all three compounds, the spectra shown in Figures 3 and 4 (as well as the lifetime differences of the ~525 nm band) indicate the presence of a different type of excited state, particularly in the **GdAu** system, where the two emission bands at 612 and 525 nm show substantially different excitation profiles (Figure 4). The low energy band displays a rather broad excitation profile, while a much narrower band maximizes at 387 nm (Figure 4b) when monitoring the emission at 525 nm. Also, the excitation band maximizes in the region where the spectral profile in Figure 4a is minimal, clearly suggesting the absence of coupling between the two profiles. However, the optical dilution of **GdAu** in the excitation wavelength region is not known. Hence, the reported excitation profiles and maxima in Figure 4 are based on the assumption that the optical density is low in this region.

Moreover, the lifetime values for the higher energy emission in **GdAu** is shorter by a factor of 10 relative to **Gd(terpy)**. Therefore, the d^{10} transition metals appear to have a definite role in influencing the overall PL properties. However, comparison of the spectral profiles clearly shows that the manner in which the two metals (Au vs Ag) influence the spectra is different. For example, **GdAu** shows a structured emission at 77 K, which is absent in **GdAg**. The lack of a similar profile in the **GdAg** system both in terms of the time dependent profile (Figure 9) and/or the excitation dependent steady state emission suggests that the Au···Au interaction is involved in the transition.[54]

Excitation spectra in the **GdAu** system are well structured, indicating vibronic coupling to the electronic transition. The emission and excitation behaviors suggest that the excited state consists of a large contribution from the terpy ligand orbitals, while the ground state responsible for the transition involves contributions from gold-based metal orbitals. Reports on several other d^{10} and terpyridine complexes make a similar assignment, where a MLCT transition has been noted as the primary transition in the visible region.[55] As mentioned earlier, (TPA)AuBr[44] displays similar spectral characteristics overall. In that system, each of the two excited states (metal-centered and LMCT) provide distinct excitation and emission profiles and are distinguished on the basis of their spectral variations and lifetime differences,[44] again similar to the situation for **GdAu**. However, it is obvious that additional investigations might be necessary on plausible model compounds, such as the lanthanum or lutetium analogs, for definitive support of this assignment. Finally, the assignment of the weak emission band with vibronic coupling at ~385 nm (Figure 5a) is straightforward, as it is consistent with a ligand-centered $\pi-\pi^*$ transition usually observed in terpy systems.[48−50,55,56]

Quantum Yield (QY) Studies. Quantum yield measurements on these systems reveal the extent of the quantum efficiency related to the excimer emission. Such evaluations are important since strong red-light emitting materials have potential applications in many commercial, industrial, and medicinal applications. For example, red emitting materials are widely used in phototherapy because of the penetrating ability of the long wavelength red light through the human body.[57] The fabrication of new PL materials with the capability to emit red-light under proper conditions continues as a scientific pursuit[58] ever since the discovery of the first successful red-light-emitting diode (LED) in the early 1960s. Moreover, red emitting fluorescent powders are one of the basic fluorescent additives in preparing white LED fluorescent lamps.[58]

The QY of the red excimer emission appears to depend on the wavelength used to excite the sample. Excitation at 365 nm yields a QY value of 1.4% for the **GdAu** compound, whereas excitation at 420 nm almost doubles the yield to 2.7%.

On the basis of these values, the radiative and nonradiative rate constants, k_r and k_{nr}, respectively, were calculated[55] using eqs 1 and 2 and the results presented in Table 3:

$$k_r = \frac{\phi_{sp}}{\tau_{obs}} \quad (1)$$

$$k_{nr} = \left(\frac{1}{\tau_{obs}} - k_r\right) \quad (2)$$

where, ϕ_{sp} is the quantum yield and τ_{obs} is the measured lifetime.

The radiative rate constants, k_r, for **GdAu** and **GdAg** are 17.7 and 84.4 s^{-1}, respectively. As shown in Table 3, the nonradiative components (k_{nr}) are 638 and 685 s^{-1} for **GdAu** and **GdAg**, respectively. These values indicate that nonradiative processes are dominant when compared with the radiative routes. As a result, modification of the structural features is needed to enhance the radiative component exhibited in these systems and therefore increase the likelihood of any practical applications.

SUMMARY AND CONCLUSIONS

Structural and spectroscopic features of isostructural Gd(terpy)$(H_2O)(NO_3)_2M(CN)_2$ (M = Au, Ag) complexes are reported. Both compounds luminesce with a characteristic red-orange color upon excitation with UV light. Additionally, **GdAu**, but not **GdAg**, displays a broad green emission when excited in the near UV. Structural studies reveal the presence of M···M distances larger than the sum of van der Waals radii and π-stacking of the terpy ligands. The Au···Au (3.5054(4) Å) and the Ag···Ag (3.6553(5) Å) interactions appear to be too weak to provide the low energy red emission; however, the green emission in **GdAu** presumably results from a LMCT transition primarily from the aurophilic interaction. The combined experimental evidence indicates that the unusual red-orange emission exhibited in both compounds originates from an excited state involving exciplexes formed from the intermolecular π-stacking of the terpy ligands.

ASSOCIATED CONTENT

Supporting Information

X-ray crystallographic data for **GdAu** and **GdAg** in CIF format. X-ray crystallographic data for **GdAu** and **GdAg** and PL spectra of **Gd(terpy)**. This material is available free of charge via the Internet at http://pubs.acs.org.

AUTHOR INFORMATION

Corresponding Author

*E-mail: rsykora@southalabama.edu (R.E.S.), zassefa@ncat.edu (Z.A.). Phone: (251)460-7422 (R.E.S.), (336)285-2255 (Z.A.).

Notes

The authors declare no competing financial interest.

■ ACKNOWLEDGMENTS

The authors gratefully acknowledge the National Science Foundation for their generous support (NSF-CAREER grant to R.E.S., CHE-0846680). Z.A. acknowledges support from the NOAA Educational Partnership Program award number NA06OAR4810187 to NCAT State University and support from the donors of the ACS Petroleum Research fund (ACS-PRF).

■ REFERENCES

(1) Fiddler, M. N.; Begashaw, I.; Mickens, M. A.; Collingwood, M. S; Assefa, Z.; Bililign, S. *Sensors* **2009**, *9*, 10447−10512.
(2) Kutal, C. *Coord. Chem. Rev.* **1990**, *99*, 213−252.
(3) Horváth, O. *Coord. Chem. Rev.* **1994**, *135/136*, 303−324.
(4) Ford, P. C.; Vogler, A. *Acc. Chem. Res.* **1993**, *26*, 220−226.
(5) Forward, J. M.; Fackler, J. P., Jr.; Assefa, Z. In *Optoelectronic Properties of Inorganic Compounds*; Roundhill, D. M., Fackler, J. P., Jr., Eds.; Plenum Press: New York, 1999; Chapter 6.
(6) Bowmaker, G. A. Spectroscopic Methods in Gold Chemistry. In *Gold: Progress in Chemistry, Biochemistry and Technology*; Chapter 21, Schmidbaur, H., Ed.; Wiley: Chichester, NY, 1999.
(7) Patterson, H. H.; Kanan, S. M.; Omary, M. A. *Coord. Chem. Rev.* **2000**, *208*, 227−241.
(8) (a) Sharpe, A. G. *The Chemistry of Cyano Complexes of the Transition Metals*; Academic Press: London, 1976. (b) Katz, M. J.; Sakai, K.; Leznoff, D. B. *Chem. Rev.* **2008**, *37*, 1884−1895. (c) Korcok, J. L.; Katz, M. J.; Leznoff, D. B. *J. Am. Chem. Soc.* **2009**, *131*, 4866−4871. (d) Geisheimer, A. R.; Huang, W.; Pacradouni, V.; Sabok-Sayr, S. A.; Sonier, J. E.; Leznoff, D. B. *Dalton Trans.* **2011**, *40*, 7505−7516.
(9) (a) Mason, W. R. *J. Am. Chem. Soc.* **1973**, *95*, 3573−3581. (b) Mason, W. R. *J. Am. Chem. Soc.* **1976**, *98*, 5182−5187.
(10) Rawashdeh-Omary, M. A.; Omary, M. A.; Patterson, H. H. *J. Am. Chem. Soc.* **2000**, *122*, 10371−10380.
(11) (a) Kurmoo, M.; Day, P.; Mitani, T.; Kitagawa, H.; Shimoda, H.; Yoshida, D.; Guionneau, P.; Barrans, Y.; Chasseau, D.; Ducasse, L. *Bull. Chem. Soc. Jpn.* **1996**, *69*, 1233−1240. (b) Chasseau, D.; Guionneau, P.; Rahal, M.; Bravic, G.; Gaultier, J.; Ducasse, L.; Kurmoo, M.; Day, P. *Synth. Met.* **1995**, *70*, 945−946. (c) Fujiwara, H.; Kobayashi, H. *Chem. Commun.* **1999**, 2417−2418. (d) Kurmoo, M.; Pritchard, K. L.; Talham, D. R.; Day, P.; Stringer, A. M.; Howard, J. A. K. *Acta Crystallogr.* **1990**, *B46*, 348−354.
(12) Shaw, C. F., III. The Biochemistry of Gold. In *Gold: Progress in Chemistry, Biochemistry and Technology*; Schmidbaur, H., Ed.; Wiley: Chichester, NY, 1999; Chapter 10.
(13) Elder, R. C.; Elder, K. T. U.S. Patent 5603963, 1997.
(14) Adams, M. D.; Johns, M. W.; Dew, D. W. Recovery of Gold from Ores and Environmental Aspects. In *Gold: Progress in Chemistry, Biochemistry and Technology*; Schmidbaur, H., Ed.; Wiley: Chichester, NY, 1999; Chapter 3.
(15) (a) Patterson, H. H.; Roper, G.; Biscoe, J.; Ludi, A.; Blom, N. *J. Lumin.* **1984**, *31*−*32*, 555−557. (b) Markert, J. T.; Blom, N.; Roper, G.; Perregaux, A. D.; Nagasundaram, N.; Corson, M. R.; Ludi, A.; Nagle, J. K.; Patterson, H. H. *Chem. Phys. Lett.* **1985**, *118*, 25862. (c) Assefa, Z.; DeStefano, F.; Garepapaghi, M.; LaCasce, J. Jr.; Ouellete, S.; Corson, M.; Nagle, J.; Patterson, H. H. *Inorg. Chem.* **1991**, *30*, 2868−2876. (d) Nagle, J.; LaCasce, J. Jr.; Corson, M.; Dolan, P. J. Jr.; Assefa, Z.; Patterson, H. H. *Mol. Cryst. Liq. Cryst.* **1990**, *181*, 359−366. (e) Assefa, Z.; Shankle, G.; Reynolds, R.; Patterson, H. H. *Inorg. Chem.* **1994**, *33*, 2187−2195.
(16) Omary, M. A.; Patterson, H. H. *Inorg. Chem.* **1998**, *37*, 1060−1066.
(17) Omary, M. A.; Patterson, H. H. *J. Am. Chem. Soc.* **1998**, *120*, 7696−7705.
(18) Omary, M. A.; Hall, D. R.; Shankle, G. E.; Siemiarczuk, A.; Patterson, H. H. *J. Phys. Chem. B* **1999**, *103*, 3845−3853.
(19) (a) Lowry, T. H.; Schuller-Richardson, K. *Mechanism and Theory in Organic Chemistry*; Harper & Row: New York, 1981; pp 919−925. (b) Turro, N. J. *Modern Molecular Photochemistry*; Benjamin/Cummings: Menlo Park, CA, 1978; pp 135−146. (c) Lamola, A. A. In *Energy Transfer and Organic Photochemistry*; Lamola, A. A., Turro, N. J., Eds.; Wiley-Interscience: New York, 1969; pp 54−60. (d) *The Exciplex*; Gordon, M., Ware, W. R., Eds; Academic Press: New York, 1975. (e) Kopecky, J. *Organic Photochemistry: A Visual Approach*; VCH: New York, 1991; pp 38−40. (f) Michl, J.; Bonačić-Koutecký, V. *Electronic Aspects of Organic Photochemistry*; Wiley: New York, 1990; pp 274−286.
(20) Horváth, A.; Stevenson, K. L. *Coord. Chem. Rev.* **1996**, *153*, 57−82.
(21) (a) Bailey, J. A.; Hill, M. G.; Marsh, R. E.; Miskowski, V. M.; Schaefer, W. P.; Gray, H. B. *Inorg. Chem.* **1995**, *34*, 4591−4599. (b) Miskowski, V. M.; Houlding, V. H. *Inorg. Chem.* **1989**, *28*, 1529−1533.
(22) (a) Chan, C.-W.; Lai, T.-F.; Che, C.-M.; Peng, S.-M. *J. Am. Chem. Soc.* **1993**, *115*, 11245−11253. (b) Kunkely, H.; Vogler, A. *J. Am. Chem. Soc.* **1990**, *112*, 5625−5627.
(23) (a) Stevenson, K. L.; Dhawale, R. S.; Horváth, A.; Horváth, O. *J. Phys. Chem. A* **1997**, *101*, 3670−3676. (b) Stevenson, K. L.; Knorr, D. W.; Horváth, A. *Inorg. Chem.* **1996**, *35*, 835−839. (c) Horváth, A.; Wood, C. E.; Stevenson, K. L. *Inorg. Chem.* **1994**, *33*, 5351−5354. (d) Horváth, A.; Wood, C. E.; Stevenson, K. L. *J. Phys. Chem.* **1994**, *98*, 6490−6495. (e) Horváth, A.; Stevenson, K. L. *Inorg. Chem.* **1993**, *32*, 2225−2227.
(24) (a) Stacy, E. M.; McMillin, D. R. *Inorg. Chem.* **1990**, *29*, 393−396. (b) Palmer, C. E. A.; McMillin, D. R.; Kirmaier, C.; Holten, D. *Inorg. Chem.* **1987**, *26*, 3167−3170.
(25) (a) Ayala, N. P.; Demas, J. N.; DeGraff, B. A. *J. Phys. Chem.* **1989**, *93*, 4104−4109. (b) Ayala, N. P.; Demas, J. N.; DeGraff, B. A. *J. Am. Chem. Soc.* **1988**, *110*, 1523−1529.
(26) Ayala, N. P.; Flynn, C. M. Jr.; Sacksteder, L.; Demas, J. N.; DeGraff, B. A. *J. Am. Chem. Soc.* **1990**, *112*, 3837−3844.
(27) (a) Yamamoto, S.; Doi, M. *J. Chem. Soc., Faraday Trans.* **1997**, *93*, 1309−1312. (b) Takahashi, O.; Sotowa, C.; Saito, K.; Ahmed, O.; Yamamoto, S. *J. Chem. Soc., Faraday Trans.* **1995**, *91*, 3794−3798.
(28) (a) Clodfelter, S. A.; Doede, T. M.; Brennan, B. A.; Nagle, J. K.; Bender, D. P.; Turner, W. A.; LaPunzia, P. M. *J. Am. Chem. Soc.* **1994**, *116*, 11379−11386. (b) Nagle, J. K.; Brennan, B. A. *J. Am. Chem. Soc.* **1988**, *110*, 5931−5932.
(29) Pettijohn, C. N.; Chuong, B.; Nagle, J. K.; Vogler, A. *Coord. Chem. Rev.* **1998**, *171*, 85−92.
(30) (a) Colis, J. C. F.; Staples, R.; Tripp, C.; Labrecque, D.; Patterson, H. H. *J. Phys. Chem. B* **2005**, *109*, 102−109. (b) Rawashdeh-Omary, M. A.; Omary, M. A.; Patterson, H. H.; Fackler, J. P. Jr. *J. Am. Chem. Soc.* **2001**, *123*, 11237−11247.
(31) (a) Rawashdeh-Omary, M. A.; Omary, M. A.; Shankle, G. E.; Patterson, H. H. *J. Phys. Chem. B* **2000**, *104*, 6143−6151. (b) Rawashdeh-Omary, M. A.; Larochelle, C. L.; Patterson, H. H. *Inorg. Chem.* **2000**, *39*, 4527−4534.
(32) Yersin, H.; Trumbach, D.; Strasser, J.; Patterson, H. H.; Assefa, Z. *Inorg. Chem.* **1998**, *37*, 3209−3216.
(33) Stevenson, K. L.; Bell, P. B.; Watson, R. E. *Coord. Chem. Rev.* **2002**, *229*, 133−146.
(34) Kyle, K. R.; Ford, P. C. *J. Am. Chem. Soc.* **1989**, *111*, 5005−5006.
(35) Stevenson, K. L.; Bell, P. B.; Horváth, O.; Horváth, A. *J. Am. Chem. Soc.* **1998**, *120*, 4234−4235.
(36) Stevenson, K. L.; Bell, P. B.; Dhawale, R. S.; Horváth, O.; Horváth, A. *Radiat. Phys. Chem.* **1999**, *55*, 489−496.
(37) (a) Maynard, B. A.; Smith, P. A.; Ladner, L.; Jaleel, A.; Beedoe, N.; Crawford, C.; Assefa, Z.; Sykora, R. E. *Inorg. Chem.* **2009**, *48*, 6425−6435. (b) Maynard, B.; Kalachnikova, K.; Sykora, R. E.; Whitehead, K.; Assefa, Z. *Inorg. Chem.* **2008**, *47*, 1895−1897.
(38) (a) Maynard, B. A.; Smith, P. A.; Jaleel, A.; Ladner, L.; Sykora, R. E. *J. Chem. Crystallogr.* **2010**, *40*, 616−623. (b) Smith, P. A.; Stojanovic, M.; Sykora, R. E. *Acta Crystallogr.* **2010**, *E66*, m1619−m1620.
(39) *CrysAlis PRO*; Oxford Diffraction Ltd.: Abington, England, 2010.
(40) Sheldrick, G. M. *Acta Crystallogr.* **2008**, *A64*, 112−122.

(41) (a) Leverd, P. C.; Charbonnel, M.-C.; Dognon, J.-P.; Lance, M.; Nierlich, M. *Acta Crystallogr.* **1999**, *C55*, 368−370. (b) Semenova, L. I.; White, A. H. *Aust. J. Chem.* **1999**, *52*, 507−517.
(42) Sykora, R. E.; Assefa, Z. A. Unpublished results.
(43) (a) Ahrland, S.; Noren, B.; Oskarsson, A. *Inorg. Chem.* **1985**, *24*, 1330−1333. (b) Barrow, M.; Burgi, H.; Johnson, D.; Venanzi, L. *J. Am. Chem. Soc.* **1976**, *98*, 2356−2357. (c) Janiak, C.; Hoffmann, R. *Inorg. Chem.* **1989**, *28*, 2743−2747. (d) Uson, R.; Laguna, A.; Laguna, M.; Jones, P. G.; Sheldrick, G. M. *J. Chem. Soc., Chem. Commun.* **1981**, 1097−1098. (e) Jiang, Y.; Alvarez, S.; Hoffmann, R. *Inorg. Chem.* **1985**, *24*, 749−757. (f) Mehrotra, P.; Hoffmann, R. *Inorg. Chem.* **1978**, *17*, 2187−2189. (g) Dedieu, A.; Hoffmann, R. *J. Am. Chem. Soc.* **1978**, *100*, 2074−2079. (h) Bayler, A.; Schier, A.; Bowmaker, G. A.; Schmidbaur, H. *J. Am. Chem. Soc.* **1996**, *118*, 7006−7007.
(44) Assefa, Z.; McBurnett, B. G.; Staples, R. J.; Fackler, J. P.; Assmann, B.; Angermaier, K.; Schmidbaur, H. *Inorg. Chem.* **1995**, *34*, 75−83.
(45) Assefa, Z.; McBurnett, B. G.; Staples, R. J.; Fackler, J. P. *Inorg. Chem.* **1995**, *34*, 4965−4972.
(46) Toronto, D. V.; Weissbart, B.; Tinti, D. S.; Balch, A. L. *Inorg. Chem.* **1996**, *35*, 2484−2489.
(47) Fink, D. W.; Pivnichny, J. V.; Ohnesorge, W. E. *Anal. Chem.* **1969**, *41*, 833−834.
(48) Yoshikawa, N.; Yamabe, S.; Kanehisa, N.; Takashima, H.; Tsukahara, K. *J. Phys. Org. Chem.* **2009**, *22*, 410−417.
(49) Nakamoto, K. *J. Phys. Chem.* **1960**, *64*, 1420−1425.
(50) Berkovic, G. E.; Ludmer, Z. *Chem. Phys. Lett.* **1983**, *100*, 102−104.
(51) (a) Ferguson, J. *J. Chem. Phys.* **1958**, *28*, 765−768. (b) Stevens, B. *Spectrochim. Acta* **1962**, *18*, 439−448.
(52) (a) Hergold, A.; Popovic, Z.; Matkovic-Calogovic, D. *Acta Crystallogr.* **1996**, *C52*, 3154−3157. (b) Balzani, V.; Juris, A.; Venturi, M.; Campagna, S.; Serroni, S. *Chem. Rev.* **1996**, *96*, 759−833. (c) Cances, E.; Mennucci, B.; Tomasi, J. *J. Chem. Phys.* **1997**, *107*, 3032−3041. (d) Kochel, A. *Acta Crystallogr.* **2006**, *E62*, m37−m38.
(53) Fink, D. W.; Ohnesorge, W. E. *J. Phys. Chem.* **1970**, *74*, 72−77.
(54) (a) Omary, M. A.; Webb, T. R.; Assefa, Z.; Shankle, G. E.; Patterson, H. H. *Inorg. Chem.* **1998**, *37*, 1380−1386. (b) Singh, K; Long, J. R.; Stavropoulos, P. *J. Am. Chem. Soc.* **1997**, *119*, 2942−2943. (c) Kim, Y.; Seff, K. *J. Am. Chem. Soc.* **1977**, *99*, 7055−7057. (d) Kim, Y.; Seff, K. *J. Am. Chem. Soc.* **1978**, *100*, 175−180. (e) Eastland, G. W.; Mazid, M. A.; Russell, D. R.; Symons, M. C. R. *J. Chem. Soc., Dalton Trans.* **1980**, 1682−1687.
(55) (a) Shikhova, E.; Danilov, E. O.; Kinayyigit, S.; Pomestchenko, I. E.; Tregubov, A. D.; Camerel, F.; Retailleau, P.; Ziessel, R.; Castellano, F. *Inorg. Chem.* **2007**, *46*, 3038−3048. (b) Yan, C.; Chen, Q.; Chen, L.; Feng, R.; Shan, X.; Jiang, F.; Hong, M. *Aust. J. Chem.* **2011**, *64*, 104−118. (c) Polson, M. I. J.; Medlycott, E. A.; Hanan, G. S.; Mikelsons, L.; Taylor, N. L.; Watanabe, M.; Tanaka, Y.; Loiseau, F.; Passalacqua, R.; Campagna, S. *Chem.—Eur. J.* **2004**, *10*, 3640−3648.
(56) (a) Quici, S.; Marzanni, G.; Cavazzini, M.; Anelli, P. L.; Botta, M.; Gianolio, E.; Accorsi, G.; Armaroli, N.; Barigelletti, F. *Inorg. Chem.* **2002**, *41*, 2777−2784. (b) Gao, X.-C.; Cao, H.; Huang, C.-H.; Umitani, S.; Chen, G.-Q.; Jiang, P. *Synth. Met.* **1999**, *9*, 127−132.
(57) Yin, W.; Esposito, D. V.; Yang, S.; Ni, C.; Chen, J. G.; Zhao, G.; Zhang, Z.; Hu, C.; Cao, M.; Wei, B. J. *Phys. Chem. C* **2010**, *114*, 13234−13240.
(58) (a) Zhang, J.; Takahashi, M.; Tokuda, Y.; Yoko, T. *J. Ceram. Soc. Jpn.* **2004**, *112*, 511−513. (b) Guo, H.; Li, F.; Li, J.; Zhang, H. *J. Am. Ceram. Soc.* **2011**, *94*, 1651−1653. (c) Ohkita, M; Endo, A; Sumiya, K.; Nakanotani, H.; Suzuki, T.; Adachi, C. *J. Lumin.* **2011**, *131*, 1520−1524. (d) Smet, P. F; Parmentier, A. B; Poelman, D. *J. Electrochem. Soc.* **2011**, *158*, R37−R54.